RPI/CHE/NASA-5-23390-5

An Augmented Young-Laplace Model of an Evaporating Meniscus in a Micro-Channel with a High Heat Flux", J. A. Schonberg, S. DasGupta, P. C. Wayner, Jr., Manuscript submitted to the International Journal of Experimental Heat Transfer, Thermodynamics, and Fluid Mechanics

P.C. Wayner, Jr., and J. Plawsky
The Isermann Department of Chemical Engineering
Rensselaer Polytechnic Institute
Troy, NY 12180-3590

Prepared for

AN AUGMENTED YOUNG-LAPLACE MODEL OF AN EVAPORATING

MENISCUS IN A MICRO-CHANNEL WITH HIGH HEAT FLUX

J.A. Schonberg, S. DasGupta and P.C. Wayner, Jr.*

The Isermann Department of Chemical Engineering
Rensselaer Polytechnic Institute
Troy, New York, 12180-3590

Telephone: (518) 276-6199
Telefax: (518)276-4030

*person to whom all correspondence should be addressed.

ABSTRACT

High flux evaporation from a steady meniscus formed in a 2 μm channel is modeled using the augmented Young-Laplace equation. The heat flux is found to be a function of the long range van der Waals dispersion force which represents interfacial conditions between heptane and various substrates. Heat fluxes of $(1.3\text{-}1.6) \times 10^6$ W/m^2 based on the width of the channel are obtained for heptane completely wetting the substrate at 100°C. Small channels are used to obtain these large fluxes. Even though the real contact angle is 0°, the apparent contact angle is found to vary between 24.8° and 25.6°. The apparent contact angle, which represents viscous losses near the contact line, has a large effect on the heat flow rate because of its effect on capillary suction and the area of the meniscus.

The interfacial heat flux is modeled using kinetic theory for the evaporation rate. The superheated state depends on the temperature and the pressure of the liquid phase. The liquid pressure differs from the pressure of the vapor phase due to capillarity and long range van der Waals dispersion forces which are relevant in the ultra thin film formed at the leading edge of the meniscus. Important pressure gradients in the thin film cause a substantial apparent contact angle for a completely wetting system. The temperature of the liquid is related to the evaporation rate and to the substrate temperature through the steady heat conduction equation. Conduction in the liquid phase is calculated using finite element analysis except in the vicinity of the thin film. A lubrication theory solution for the thin film is combined with the finite element analysis by the method of matched asymptotic expansions.

KEYWORDS: Micro heat transfer device, thin liquid films, evaporation, augmented Young-Laplace equation, contact angle, finite element analysis.

INTRODUCTION

An understanding of the heat transfer characteristics of an evaporating extended meniscus is of central importance to the design of many small heat pipes and thermosyphons based on interfacial phenomena. Herein, a portion of the inverted meniscus system presented in Fig. 1 is analyzed. Using a finite element procedure, kinetic theory and the augmented Young-Laplace equation of capillarity, the magnitude of the heat flow rate of a steady evaporating "inverted meniscus" is numerically evaluated. The long term objective is to determine the maximum heat sink capability of the inverted meniscus heat pipe. Since resistances associated with fluid flow and evaporation change the shape of the evaporating meniscus, the immediate objective is to evaluate the effect of viscous stresses on the meniscus profile. Future research will incorporate the results of the two-dimensional analysis presented below in a three dimensional study.

For perspective, the evolution of the present problem can be briefly traced as follows. In 1972, Raiff and Wayner [1, 2] experimentally and theoretically studied a porous liquid flow control design that was a precursor to the inverted meniscus heat pipe studied by Saaski [3]. These studies demonstrated that the evaporating inverted meniscus was controlled by the heat transfer characteristics of the contact line region. In a complementary theoretical study in 1972, Potash and Wayner [4] described an evaporating extended meniscus which consisted of an intrinsic meniscus and a thin film extending beyond the apparent contact line of the intrinsic meniscus. The two regions are designated in the inverted meniscus design presented in Fig. 2. The portion of the extended meniscus that was described using the classical equation of capillarity was called the intrinsic meniscus. The complementary adjacent thin film was described using the disjoining pressure concept of Derjaguin [5, 6]. In 1980, Moosman and Homsy [7] presented a procedure which included the effect of conduction in the liquid and demonstrated that the relative size of this resistance was substantial. A review of the extensive literature and recent data that leads to the current analysis was

recently presented by Wayner and coworkers [8-10]. Recently, Wu and Peterson studied a wickless micro heat pipe which had outer dimensions of 1 mm x 1 mm x 57 mm. Since the fluid had a finite contact angle, they used the classical equation of capillarity to describe the internal fluid dynamics [11]. Xu and Carey used a completely wetting fluid to study film evaporation from a micro-grooved surface with grooves 64 μm wide and 190 μm deep [12]. Although a small evaporating meniscus could be a large heat sink, this result has not been conclusively demonstrated because of the complex physicochemical phenomena present in the microscopic contact line region.

Existing models apply lubrication theory to the thin film to relate the flow to the pressure gradient, apply the augmented Young-Laplace equation to relate the pressure in the film to its shape through disjoining pressure and capillarity, and link the gradient of flow to the evaporation flux from the film. The flux is linked to the **local** thermodynamic conditions of the liquid phase relative to the vapor phase. Use of the augmented Young-Laplace equation is strongly supported by the fact that it agrees with the disjoining pressure isotherm for the extreme of a flat film and with the Young-Laplace equation for a thick film. Furthermore, it provides a convenient mathematical resolution of the breakdown of lubrication models based solely on capillary pressure gradients as film thickness approaches zero. In the experimental studies of Wayner and coworkers [8, 9] with small superheating, the analysis provides a theoretical solution which gives good to excellent agreement with the thin flat film data and with the capillary dominated thicker (relatively isobaric) portion of the film. There is only one adjustable parameter and its behavior is reasonable although its absolute value is not known independently. Agreement is more approximate in the transitional portion of the films. While the form of the kinetic theory based mass transfer model of evaporation is supported, the magnitude of the evaporation coefficient is unknown.

The extended meniscus in the channel also has a thicker portion in which lubrication theory is not valid. In this work, the two regions are analyzed

separately and the numerical results are joined together in the framework of the method of matched asymptotic expansions to obtain the steady state heat flow rate for the complete extended meniscus. Previously, the meniscus in a heat pipe evaporator was studied by Stephan and Busse [13]. In their method the meniscus shape and heat transfer problem in the micro region and the two dimensional heat conduction problem in the macro region were solved. Conduction in the solid substrate was also included. Since the solution of each problem was needed as input for the other one, an iterative procedure was used. Recent work by Swanson and Peterson [14] shed considerable light into the critical mechanisms required for proper heat pipe operation. Their thermodynamic model provided insights into the behavior of the extended meniscus in capillary structures. It included the effects of axial temperature difference, changes in local interface curvature, Marangoni effects and disjoining pressure.

MATHEMATICAL FORMULATION

Consider a steady liquid meniscus in a two dimensional channel as shown in Figs. 1-3. The liquid is superheated relative to the vapor phase by the solid surfaces (the slot walls) and so evaporates. A fresh supply is drawn into the channel to sustain steady evaporation. Following Wayner and coworkers [8-10] the evaporation flux is modeled as

$$\dot{m} = a(T_{lv} - T_v) + b(P_l - P_v) \tag{1}$$

where a and b depend only on the physical properties of the liquid. The vapor phase is assumed to be uniform, having temperature T_v and pressure P_v. There is only one component, both phases are pure. The interfacial temperature of the liquid T_{lv} and its pressure P_l are in general functions of position.

The coefficients are

$$a = C\left(\frac{M}{2\pi RT_{lv}}\right)^{1/2}\left(\frac{P_v M \Delta h_m}{RT_v T_{lv}}\right) \tag{2}$$

$$b = C \left(\frac{M}{2\pi RT_{lv}}\right)^{1/2} \left(\frac{V_l P_v}{RT_{lv}}\right) \tag{3}$$

where C is the accommodation coefficient with an ideal value of 2.0, M is the molecular weight, R is the universal gas constant, P_v is the *bulk* vapor pressure of the evaporating material at temperature T_{lv}, V_l is the molar volume of the bulk material, Δh_m is the enthalpy of vaporization of the material per unit mass at temperature T_{lv}. In Eq.(1), evaporation is promoted by a superheat and hindered by a low liquid film pressure. If the temperature differences are small compared to the absolute temperature, the known substrate temperature, T_s, may be substituted for the unknown T_{lv} in the coefficients. The quantity of interest is the heat sink per unit pore depth, Q,

$$Q \equiv \Delta h_m \int_C \dot{m} \, dl \tag{4}$$

where C represents an integration over the length of the liquid-vapor interface. The liquid pressure at the interface, P_l, is related to the flow of liquid through the Navier Stokes and continuity equations. It is also related to the unknown interface shape and the vapor phase pressure, P_v, through capillarity and long range intermolecular forces by the augmented Young-Laplace equation, Eq. (5).

$$P_l - P_v = -\Pi - \sigma K \tag{5}$$

with

$$\Pi = -\frac{\bar{A}}{\delta^3} \tag{6}$$

where $6\pi\bar{A}$ is the Hamaker constant (**negative** for a completely wetting liquid), $\bar{A}$ is the dispersion constant, $\delta(x)$ is the film thickness, K is the curvature and σ is the surface tension. The first term on the rhs of Eq. (5) is called the disjoining pressure, Π, and it represents the change in the body force on the liquid due to the long range van der Waals forces between the liquid and solid over a narrow range

of thicknesses. Herein, a "pressure jump" model is used to account for both the disjoining pressure and capillarity. The disjoining pressure is really a model of the film thickness dependent intermolecular force field. The vapor is assumed to be pure. These forces are relevant in the very thin portions of the liquid phase. The temperature T_{lv} is related to the constant wall temperature T_s through the steady diffusion equation, convective effects taken to be negligible. The liquid is assumed to completely wet the pure wall; forming a **microscopic** contact angle of $0°$. Therefore, a portion of the liquid phase may be analyzed with lubrication theory due to the small slope. In this portion the natural length scale is the thickness of the thin film whereas in the rest of the liquid phase the natural length scale is the width of the channel, W. The radical divergence of these length scales suggests analysis with matched asymptotic expansions.

Lubrication Region, Q_{lub}

The literature provides relationships which are the building blocks for the following lubrication model of the evaporating thin film portion [see e.g., 8-10]. The liquid pressure at the interface, P_l , is related to the vapor phase pressure, P_v, by Eqs. (5) and (6). The curvature is simply the second derivative of the film thickness with distance along the substrate. Lubrication theory for a slightly tapered film relates the mass flow rate in the thin film to the pressure gradient in the direction of flow:

$$\Gamma(x) = \frac{-\delta^3}{3v} \frac{d}{dx} (P_l)$$

(7)

where $\Gamma(x)$ is the mass flow rate and v is the kinematic viscosity. These two equations demonstrate that the mass flow rate, $\Gamma(x)$, is a function of the thin film shape, $\delta(x)$. The evaporative flux, $\dot{m}$, is modeled according to Eq. (1).

Following Moosman and Homsy [7], the one dimensional conduction heat transfer solution for the film is used to eliminate T_{lv} in favor of T_s:

$$\overset{\bullet}{m} = \frac{1}{1 + \frac{a\Delta h_m}{k}\delta} [a(T_s - T_v) + b(-\Pi - \sigma K)] \qquad (8)$$

where k is the thermal conductivity of the liquid. This equation clearly demonstrates the substantial effect of film thickness on the evaporation rate. **Therefore, both fluid flow and evaporation depend on the same intermolecular force field which is a function of the film profile.**

Using a steady state material balance, the evaporative flux is

$$\frac{\partial \Gamma}{\partial x} = -\overset{\bullet}{m} \qquad (9)$$

The coupled differential equations are found to be Eq. (5) and the following combination of Eqs. (7), (8), and (9):

$$\frac{1}{3v}\frac{d}{dx}\left(\delta^3 \frac{dP_l}{dx}\right) = \frac{1}{1 + \frac{a\Delta h_m}{k}\delta} [a\Delta T + b(-\Pi - \sigma K)] \qquad (10)$$

where $\Delta T = T_s - T_v$.

The above equations are satisfied by the interline film thickness:

$$\delta_0 = \left(\frac{-\bar{A}\,b}{a\,(T_s - T_v)}\right)^{1/3} \qquad (11)$$

which provides the farfield condition

$$\delta \to \delta_0, \qquad x \to -\infty$$

These equations have been previously combined and solved numerically for the film thickness profile and the evaporation rate, $\Gamma(x)$ by Wayner and coworkers [8,9]. In this work, the Adams method solver was used to find a solution satisfying a second farfield condition

$$\frac{d\delta}{dx} \to \tan\theta_E \qquad x \to \infty \qquad (12)$$

where the effective or macroscopic apparent contact angle, θ_E , is thus defined. This quantity depends only on the physical properties of the liquid, the dispersion constant, $\bar{A}$, and the temperature difference $(T_s - T_v)$. We note that the apparent contact angle, θ_E , for this completely wetting system represents the viscous losses in the extremely thin portion of the meniscus. The contribution from the thin film lubrication region, Q_{lub}, to the total heat sink, Q, was calculated from $\Gamma(x)$. The solution for the profile , $\delta(x)$, which is schematically presented in Fig. 4, is the leading order approximation of the interface shape in the lubrication region.

Macroscopic Region, Q_{intr}

The characteristic length of the macroscopic region is the channel width W. The characteristic fluid velocity may be estimated from Eq.(1) as

$$V = a (T_S - T_V) / \rho \tag{13}$$

which is an upper bound. Using a viscous scaling appropriate for a small channel, the pressure change over a length W due to this flow is scaled as

$$\Delta P = a (T_S - T_V) v / W \tag{14}$$

The capillary pressure jump at the interface is scaled as

$$\Delta P_C = \sigma / (W/2) \tag{15}$$

For the case of interest the viscous pressure scale, ΔP, is much smaller than the capillary pressure scale, ΔP_C, by three orders of magnitude. Therefore the changes in the liquid pressure P_l from place to place on the liquid vapor interface due to viscous flow in the macroscopic region are utterly insignificant in comparison to the capillary pressure jump. Therefore, the leading order approximation of the curvature of the liquid vapor interface must be a constant. Thus, the interface is described by a section of a circle. This interface has an asymptotic form valid near a channel wall which is illustrated in Fig. 5.

Consider the circular arc:

$$(x - x_0)^2 + \left(y - \frac{W}{2}\right)^2 = R^2 \tag{16}$$

centered around a point located midway between the channel walls as shown in Fig. 5. The walls are described by the planes $y = 0$ and $y = W$. This arc is analyzed near $y = 0$ with a Taylor expansion to yield

$$y = \frac{2x}{W} \sqrt{R^2 - \frac{W^2}{4}} + O(x^2/W) \qquad x \to 0 \tag{17}$$

Since the lubrication equation is translationally invariant with respect to x, the farfield form of the lubrication solution, Equation (12), can be written as

$$\delta_{lub} \to x \tan \theta_E \qquad x \to \infty \tag{18}$$

Therefore, if R is chosen to be

$$R = \frac{W}{2} \frac{1}{\cos \theta_E} \tag{19}$$

the outer limit of the lubrication solution matches the inner limit of the macroscopic solution. Therefore, the shape of the meniscus is defined by the pore geometry and the effective contact angle θ_E.

The contribution of the macroscopic solution in the intrinsic region, Q_{intr}, to the total heat sink, Q, is found by solving

$$\nabla^2 T = 0 \tag{20}$$

$T = T_s$ on the channel walls

$-k \dfrac{\partial T}{\partial n} = 0$ on the truncation segments and on a bounding

surface through the liquid phase, well removed from the meniscus.

$-k \dfrac{\partial T}{\partial n} = a(T - T_v) - b \dfrac{\sigma}{R}$ on the liquid vapor interface where the outward unit normal vector is used.

There is a singularity where the circular arc intersects the channel wall which can be avoided by using the lubrication solution. The numerical procedures to accomplish this are discussed below.

The steady state heat equation was solved by finite element analysis. The singularity was handled by truncating the macroscopic region at a finite film thickness as shown in Fig. 6b. Since heat transfer in the lubrication region is one dimensional and perpendicular to the channel walls, the truncation surfaces were taken to be insulated. Even though the slot is semi-infinite in the "x" direction, heat transfer was anticipated only within two or three channel widths of the interface. Therefore, the domain was terminated with an insulated surface which appears on the right hand side of Fig 6a. Geometric modeling of the boundaries and mesh generation were performed with software developed at the Scientific Computation Research Center at Rensselaer. One of the meshes used is shown in Figs. 6a and b with magnification of the smaller scale portions of the liquid phase. Finite element analysis was performed with ABAQUS and a user defined element. The effect of pressure on $\dot{m}$ was estimated to be negligible in the macroscopic region. The macroscopic contribution to the heat sink Q was obtained by integration using the values of T at the mesh nodes on the boundary.

The dimensionless interfacial temperature is displayed as a function of the dimensionless distance along the channel wall in Fig. 7. A dimensionless temperature of 1.0 corresponds to the substrate temperature T_s at a film thickness of δ_o, whereas a dimensionless value of 0 corresponds to the vapor temperature T_v. In the macroscopic region, the interfacial mass flux can be obtained using these results with Eq. (1) while neglecting the effect of pressure. The lubrication region ends where the film thickness is roughly 20-30 times δ_o. The scaling of distance is shown in Fig. 6a where a dimensional distance of 2 μm is equal to a scaled distance of 4. The macroscopic region begins at -5.968. Note the mesh and model in Figs. 6a and b corresponds to the results displayed in Fig. 7.

Two meshes were tested in a sample calculation: a fine mesh and a coarse mesh. The variation in the line heat sink was only 0.1%. The element edges in the fine mesh are approximately 60% of the length of the element edges in the coarse mesh. Two cutoffs were also studied in a sample computation. The cutoffs were at +6 and +3 units (defined by the coordinate system displayed in Fig. 6a). The difference in the macroscopic line sink was $2 \ (10^{-3})\%$.

DISCUSSION

The results for various values of the modified Hamaker constant are given in Table 1. The range of Hamaker values represent a clean silicon surface at the higher value and a contaminated surface at the lower value. The intermediate value represents SiO_2. The large vapor pressure value is selected to enhance the heat flux. The predicted high average heat fluxes (based on the channel width) are apparently the result of the high vapor pressure, the large superheat, and the small channel width. The "thicker" portions of the interface are relatively inactive as shown by Figs. 7 and 6a. This is due to the assumption or rather design of a constant temperature at the channel walls and to the ease of conduction through the thinner portion of the liquid region relative to the thicker portions. Therefore, a larger channel with the same temperature difference, $T_s - T_v$, would probably have a reduced average evaporative heat flux.

The algorithm is attractive because it is not necessary to re-solve the lubrication portion if the channel width is changed, provided the basic assumptions are met (i.e., the relative width of the channel is sufficiently large.) Furthermore, an iterative computational scheme joining the finite element analysis and an ordinary differential equation solver is avoided. Both the finite element code and the differential equation solver used are standard. Finally the macroscopic apparent contact angle, θ_E, is identified as a fairly fundamental quantity of great importance affecting both the area of the meniscus and of course the capillary suction of the device. Although the variation of θ_E in these case studies is smaller than the

variation of the dispersion constant, that constant is susceptible to wide variations as shown by the fact that not all fluids completely wet a given substrate.

PRACTICAL SIGNIFICANCE AND FUTURE RESEARCH

The present work has theoretically studied the high heat transfer potential of a micro heat pipe and has showed that a heat flux of $1.3-1.6 \times 10^6$ W/m^2 is possible from a steady meniscus in a small channel. It demonstrates the importance that interline phenomena play in the emerging area of micro heat transfer. The model and the information obtained in this theoretical study have enhanced the understanding of the complex physicochemical phenomena associated with high heat flux evaporation processes and can be of importance in designing practical micro heat transfer devices. For example, since the change in the apparent contact angle due to the viscous stress in the contact line region reduces the suction potential at the base of the meniscus, the evaporating meniscus becomes unstable at a lower heat flux than would be predicted without the resistance.

Even though the calculations suggest that very high heat flux may be sustained by an evaporating meniscus in a small region, scaling up to a three dimensional device with a myriad of channels is not a trivial exercise. This is due to the fact that the pressure drop associated with the vapor removal would be substantial and a function of design. Furthermore, we note that it is experimentally very difficult to optically study the evaporating meniscus for such a high degree of superheat and the whole issue of stability at high heat flux at extremely small systems is yet to be addressed and should be considered in future studies. There are many unknowns in this small region.

CONCLUSIONS

1)   A stable evaporating meniscus with a very high heat flux based on the width of the channel is theoretically possible.

2) The simulation suggests that very high heat fluxes based on the width of the channel are associated with micron sized channels.

3) The extremely large theoretical heat fluxes in the lubrication region have not been studied experimentally.

4) A large variation in the Hamaker constant was not associated with an equally large variation in the total heat sink or the apparent contact angle.

5) The large apparent contact angle for a completely spreading system is (probably) due to large viscous stresses in the contact line region where fluid flows in an extremely thin film.

6) The apparent contact angle has a large effect on the area of the meniscus and the capillary suction of the device.

ACKNOWLEDGMENT

NOMENCLATURE

A	Hamaker constant, J
$\bar{A}$	dispersion constant, J
a	defined by Eq. (2), $kg/m^2 K s$
b	defined by Eq. (3), s/m
C	evaporation coefficient, dimensionless

Δh_m	molar heat of vaporization, J/mol
k	thermal conductivity, W/mK
K	curvature, m^{-1}
M	molecular weight, g/mol
$\dot{m}$	interfacial mass flux, $kg/m^2 s$
n	normal direction, m
P	pressure, N/m^2
Q	heat flow rate, W/m
R	gas constant, J/Kmol
R	radius of curvature, m
T	temperature, K
V	characteristic fluid velocity, m/s
V	molar volume, m^3/mol
W	channel width, m
x	coordinate distance, m
y	coordinate distance, m
δ	film thickness, m
Δ	difference
Γ	mass flow rate, kg/m
ν	kinematic viscosity, m^2/s
σ	surface tension, N/m
Π	disjoining pressure, N/m^2
ρ	density, kg/m^3
Θ	contact angle, deg

Subscripts

c	capillary
E	apparent
intr	intrinsic region
l	liquid
lub	lubrication region

o   contact line

lv   liquid-vapor interface

s   solid

Total   total of lub+intr

v   vapor

REFERENCES

1. Raiff, R.J., An Experimental and Theoretical Investigation of Suction Boiling, Ph.D. Thesis, Rensselaer Polytechnic Institute, Troy, NY, 1972.

2. Raiff, R.J., and Wayner, P.C., Jr., Evaporation from a Porous Flow Control Element on a Porous Heat Source, *Int. J. Heat Mass Transfer*, **16**, 1919-1929, 1973.

3. Saaski, E.W., Investigation of an Inverted Meniscus Heat Pipe Wick Concept, NASA CR-137,724, August 1975.

4. Potash, M, Jr., and Wayner, P.C., Jr., Evaporation from a Two-Dimensional Extended Meniscus, *Int. J. Heat Mass Transfer*, **15**, 1851-1863, 1972,

5. Derjaguin, B.V., Definition of the Concept of the Disjoining Pressure and its Role in the Statics and Kinetics of Thin Layers of Liquids, *Colloid J. of USSR* (English Translation), **17**, 191-198, 1965.

6. Derjaguin, B.V. and Churaev, N.V., Polymolecular Adsorption and Capillary Condensation in Narrow Slit Pores, *J. Colloid Interface Sci.*, **54**, 157-175, 1976.

7. Moosman, S. and Homsy, S.M., Evaporating Menisci of Wetting Fluids, *J. Colloid Interface Sci.*, **73**, 212-223, 1980.

8. Wayner, P.C., Jr., DasGupta, S., and Schonberg, J.A., Effect of Interfacial Forces on Evaporative Heat Transfer in a Meniscus, U.S. Air Force Report WL-TR-91-2061, 1991.

9. DasGupta, S., Schonberg, J.A., and Wayner, P.C., Jr., Investigation of an Evaporating Extended Meniscus Based on the Augmented Young-Laplace Equation, *J. Heat Transfer*, **115**, 201-208, 1993.

10. Wayner, P.C., Jr., The Effect of Interfacial Mass Transport on Flow in Thin Liquid Films, *Colloids and Surfaces*, **52**, 71-84, 1991.

11. Wu, D. and Peterson, G.P., Investigation of the Transient Characteristics of a Micro Heat Pipe, *J. Thermophysics*, **5**, 129-134, 1991.

12. Xu, X. and Carey, V.P., Film Evaporation from a Micro-Grooved Surface - An Approximate Heat Transfer Model and Its Comparison with Experimental Data, *J. Thermophysics*, **4**, 512-520, 1990.

13. Stephan, P. C. and Busse, C.A., Analysis of the Heat Transfer Coefficient of Grooved Heat Pipe Evaporator Walls, *Int. J. Heat Mass Transfer*, **35**(2), 383-391, 1992.

14. Swanson, L. and Peterson, G.P., The Interfacial Thermodynamics of the Capillary Structures in Micro Heat Pipes, Heat Transfer on the Microscale, HTD-Vol. 253, ASME, 45-51, 1993.
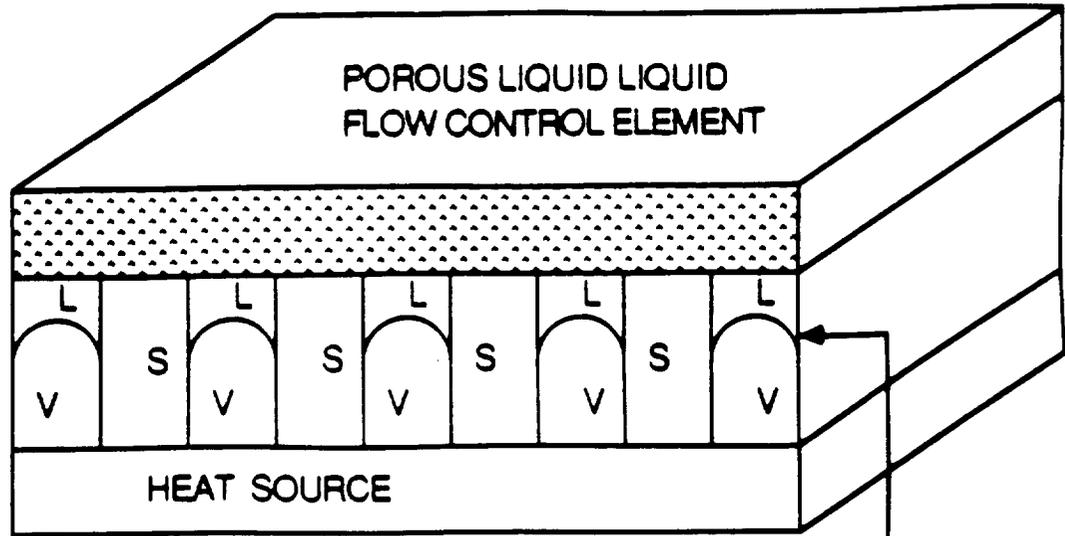
TABLE 1

SUMMARY OF HEAT PIPE CASE STUDIES

Some of the Inputs	Case: 1	Case: 2	Case: 3
$-\dot{A}$ (J)	10^{-21}	10^{-22}	10^{-23}
T (K)	373	373	373
ΔT (K)	5.19	5.19	5.19
ν (m^2/sec)	3.233×10^{-7}	3.233×10^{-7}	3.233×10^{-7}
σ (N/m)	1.247×10^{-2}	1.247×10^{-2}	1.247×10^{-2}

Calculated Values

a (kg/m^2•K•sec)	13.19	13.19	13.19
b (sec/m)	2.536×10^{-5}	2.536×10^{-5}	2.536×10^{-5}
δ_0 (Å)	7.18	3.33	1.55
$\dot{m}_{id} = a\Delta T$ (kg/m^2•sec)	68.456	68.456	68.456

Outputs

θ_E	23.75	24.80	25.43
$Q_{lub.}$ (W/m)	1.238	0.7396	0.460
$Q_{intr.}$ (W/m)	1.883	1.986	2.087
Q_{Total} (W/m)	3.121	2.726	2.547
HEAT FLUX (W/m^2) based on $W = 2 \times 10^{-6}$ m	1.5605×10^6	1.363×10^6	1.2735×10^6

LIST OF FIGURE CAPTIONS

Fig. 1.   Inverted meniscus heat pipe concept.

Fig. 2.   Schematic of Inverted Extended Evaporating Meniscus. Liquid enters through the porous flow control device that prevents the vapor from entering the liquid space above the flow control device. The passive shape of the liquid meniscus, which is a function of the transport processes and interfacial phenomena, responds to the pressure distribution in the liquid and vapor spaces which, in turn, responds to the heat flux distribution. The interfacial physics of the intermolecular force field in the extended meniscus which form the basis for the operation of this device are discussed in [4,10]. The vapor exits in the direction perpendicular to the plane of the paper.

Fig. 3.   Steady state evaporating meniscus in a channel.

Fig. 4.   Schematic diagram of solution on the scale of the adsorbed thin film thickness, δ_0. The apparent contact angle, Θ_E, is a function of the properties of the liquid, the dispersion constant, and the superheat, $T_S - T_V$.

Fig. 5.   Solution on the scale of the channel width, W. Circular arc centered at $(x_0, W/2)$. The radius R is chosen to provide the proper slope at the walls using Eq. (17).

Fig. 6a.   Finite element mesh (fine mesh) for solution of steady heat equation on macroscopic scale, each grid block (dotted lines) is 0.5 micron on edge. Detail of leading edge is shown in Figure 6b.

Fig. 6b.   Finite element mesh (fine mesh) at leading edge of the macroscopic region. The vertical edge is the truncation surface, 7.495 nm high, the rest of the interface is modeled with lubrication theory.

Fig .7   Dimensionless temperature, $(T_{lv} - T_v)/(T_s - T_v)$, versus dimensionless distance, defined in Figure 6a.

FIG 1

POROUS LIQUID LIQUID
FLOW CONTROL ELEMENT

L   L   L   L   L

S   S   S   S

V   V   V   V   V

HEAT SOURCE

V : VAPOR FLOW CHANNELS . L : LIQUID . S : SOLID FIN

[CRITICAL SHAPE CONTROLS THE HEAT FLUX
AND STABILITY OF THE PROCESS]

Fig 2

LIQUID FLOW
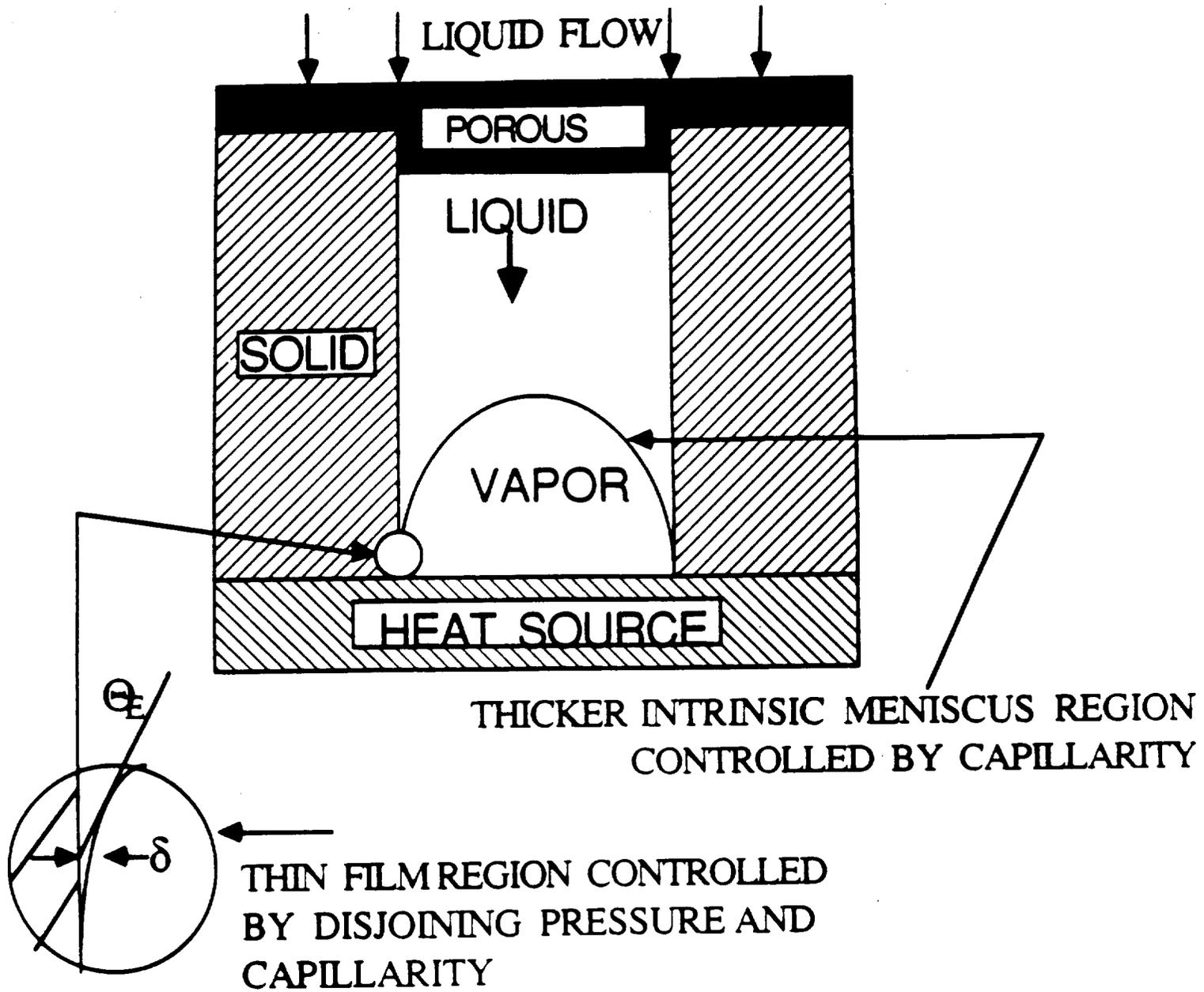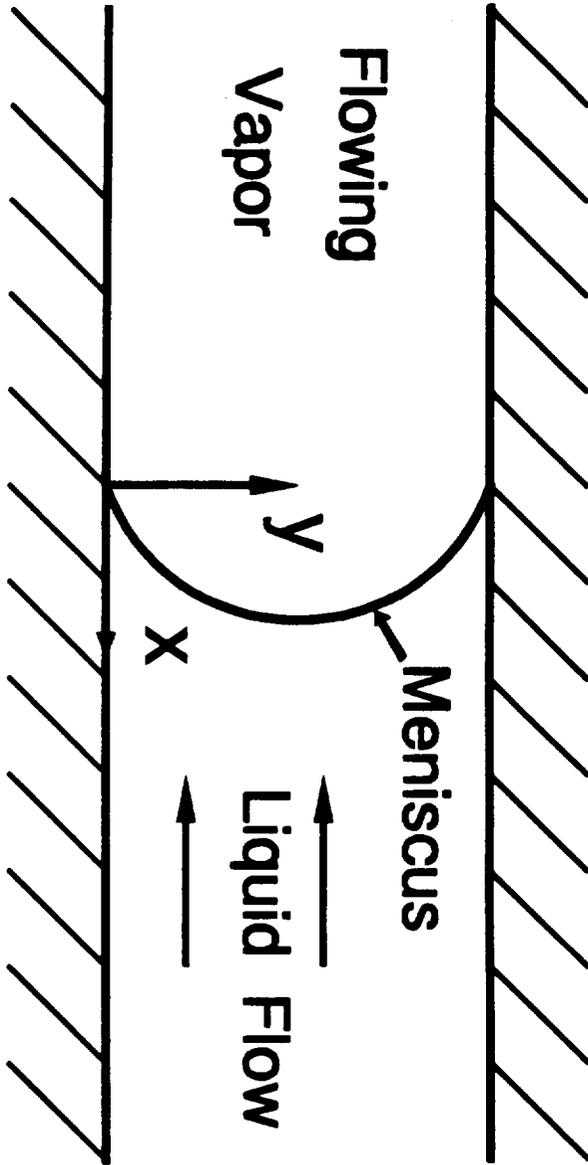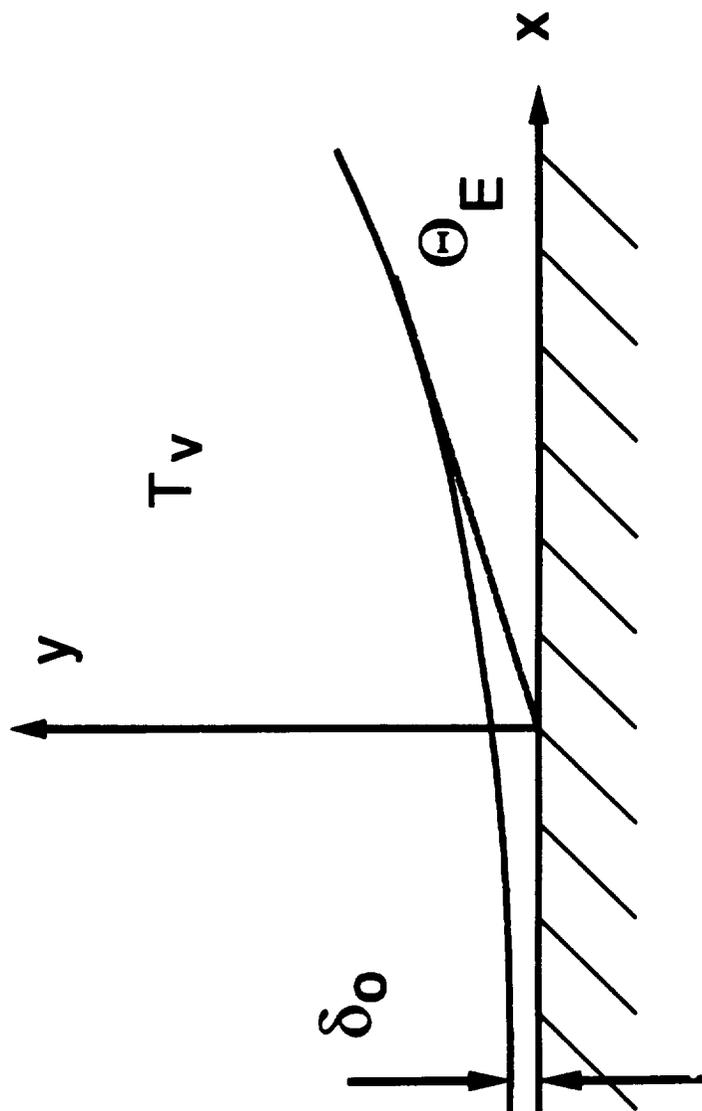
POROUS

LIQUID

SOLID

VAPOR

HEAT SOURCE

THICKER INTRINSIC MENISCUS REGION
CONTROLLED BY CAPILLARITY

θ_E

δ

THIN FILM REGION CONTROLLED
BY DISJOINING PRESSURE AND
CAPILLARITY

FIG 3

FIG 4

LUBRICATION REGION

T_v

y

x

δ_o

Θ_E

FIG 5

FIG 6b

FIG 7

PLOT OF INTERFACIAL TEMPERATURE DISTRIBUTION